공학석사학위논문

변신 바퀴를 이용한 다중 지형 이동 로봇의 설계

Wheel Transformer: A Multi-Terrain Robot with Passive Transformable Wheels

2014 년 2 월

서울대학교 대학원

기계항공공학부

김 유 석

To my family

Abstract

In this paper, the design, optimization, and performance evaluation of a new wheel-leg hybrid robot are reported. This robot utilizes a novel kind of transformable wheel for its locomotion to combine the advantages of both circular wheels and legged wheels. To minimize design complexity, this new transformable wheel's transformation process is operated passively, which eliminates the need for additional actuators. A new triggering mechanism is also employed to increase the success rate of the transformation. To maximize the climbing ability in the legged-wheel mode, the design parameters of the transformable wheel and the robot are tuned based on behavioral analyses. The performance of our new development is evaluated in terms of stability, energy efficiency, and the maximum height of the obstacle the robot can climb over. By virtue of this transformable wheel, the system could climb over an obstacle 3.25 times as tall as its wheel radius, not compromising its driving ability at 2.4 body lengths per second with the specific resistance of 0.7 on flat surfaces.

Keywords: Design, legged wheel, locomotion, mechanism, transformable, wheel.

Student number: 2012-20653

Contents

List of Figures & Tables

Fig. 15. Scenes of the robot climbing the obstacles.

Fig. 16. Design for mode change using relative motion.

Table 1. Physical specifications of the passive transformable wheel & Wheel Transformer.

1. Introduction

Small mobile robots have the advantage of being able to scout areas difficult for humans to access, such as narrow spaces within a collapsed building. In such disaster scenes, small mobile robots have exceptional potential in reconnaissance or search and rescue (SAR) missions [1][2]. An ordinary circular wheel has been a common locomotion method due to its stability and efficiency on flat surfaces. At the same time, however, small mobile robots lose their ability to climb over obstacles as the objects surrounding them grow relatively larger [3]. In other words, a circular wheel cannot climb over obstacles taller than its radius, and it is thus unsuitable for the locomotion of small robotic systems in rough terrain.

A Legged wheel was devised to overcome the limit of the climbing ability of circular wheels. A legged wheel is rimless and has several spokes, which allow it to climb obstacles taller than the radius of it. A few different types of such legged-wheel robots have been proposed. The biologically inspired hexapod runner, Whegs [4] and the quadruped, Mini Whegs [5] can climb obstacles 1.5 times as tall as their wheel radius, using rimless wheels with three spokes. RHex [6] uses six semicircular legged wheels and an open loop control to climb steps of various heights. IMPASS [7] uses three independently actuated spokes, each of which can change its length and climb

obstacles 1.7 times as tall. However, since the radius of legged wheel's rotation is inconsistent, the robot's center of mass oscillates vertically when a legged wheel drives on flat surfaces. Whegs and RHex both employ a tripod gait to minimize energy consumption [4][6].

On the other hand, locomotion systems that can alternate the leg and wheel modes have been developed to take advantage of both systems. AZIMUT displays the advantages of the leg, track, and wheel modes and selects the optimal system for a given terrain [8]. Roller-Walker can actively change the angle of wheels mounted at the end of its legs, allowing it to convert from leg mode to roller skate mode [9]. PAW can reposition and lock its wheels to change from wheel mode to leg mode [10]. PEOPLER-II uses four wheels, each of which has two bars that allow the robot to take steps on the ground in leg mode [11]. Furthermore, a mechanism that transforms wheels into legs has also been suggested. The Rolling Disk Biped (RDB) robot can walk using two legs, which can transform into wheels [12]. The retractable Wheel-Leg module is able to transform into a leg that has three linkage systems [13]. Quattroped use active transformable wheels that can be converted into semicircles like the ones already used in RHex [14]. However, these wheel-leg hybrid systems require additional actuators to switch between the two modes. As a result, the structure of the system becomes intricate, the control strategy becomes complicated,

and the manufacturing cost becomes expensive.

The overall size of a robot constrains the number of actuators that can be used in the system. It is therefore crucial to minimize the number of actuators used in small robots. Moreover, a less complicated structure provides additional benefits, such as simpler control methods and lower manufacturing cost. Small robots can demonstrate their capability especially in SAR missions, where the utilization of swarm robotic systems saves time and raises efficiency [15]. The simplicity of a robot's design significantly influences its control and performance in such situations, and even its manufacturing process. For these reasons, it is critical to devise a system that is simple yet allows a small robot to take advantage of both a wheel and a leg.

In this paper, a new kind of transformable wheel, called the passive transformable wheel, is developed (Fig. 1). Basically, it employs the advantages of both circular and legged wheels; it keeps its stability and energy efficiency when driving on even ground with its circular shape, and when it encounters an obstacle, the wheel can be transformed into a legged wheel composed of three legs. Changing from the circular wheel into the legged wheel requires only the frictional force between the wheel and an obstacle, eliminating the need for additional actuators. With its designed features, an ankle is utilized to easily trigger the transformation into a legged wheel. The design parameters of the wheel are tuned to maximize the climbing

ability. Moreover, the detail design of its simple robotic platform, Wheel Transformer, is reported, and its design parameters are also tuned to demonstrate the abilities of the passive transformable wheel.

In the following sections, we will explain the design of the passive transformable wheel in more detail. We will then optimize the design parameters for better performances. We will also present the simple robotic platform, Wheel Transformer, and tune its design parameters for stable climbing. Finally, we will conclude with a discussion about the performance of our development.

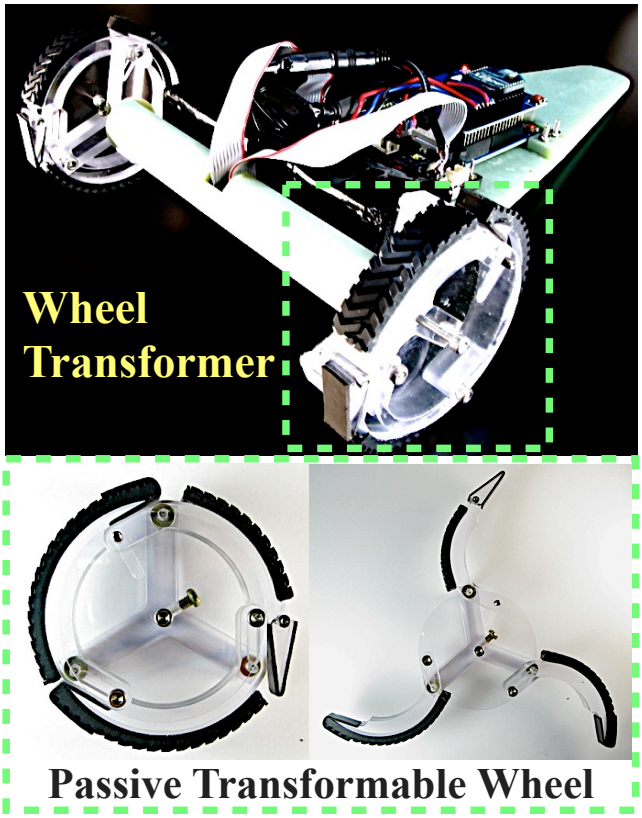

Fig. 1. A new kind of transformable wheel and Wheel Transformer.

2. Design of the passive transformable wheel

2.1 Components design for coupled legs

The basic idea of the passive transformable wheel is to segment the rim of the wheel into a number of legs and allow each leg to rotate about the revolute joint at the end of each wheel spoke as shown in Fig. 1; the number of the segmented legs is the same as the number of the spokes. Furthermore, since all the legs must unfold passively upon contact without additional actuators, the transmitting disc is used to couple the opening of the legs.

Fig. 2(a) shows the five components of the passive transformable wheel: the legs 1 and 2, the triggering leg, the transmitting disc, and the wheel spokes. The wheel spokes join the hub of the wheel to the segmented legs. The legs have a projecting handle with either a pin or a slot; one of the legs is a triggering leg with a pin that rotates the transmitting disc, and the pins on the transmitting disc rotate the other two legs. The transmitting disc has two pins and a slot separated symmetrically by 120°, forming pin-slide linkages with the legs. Fig. 2(b) shows the assembled wheel and the transformation.

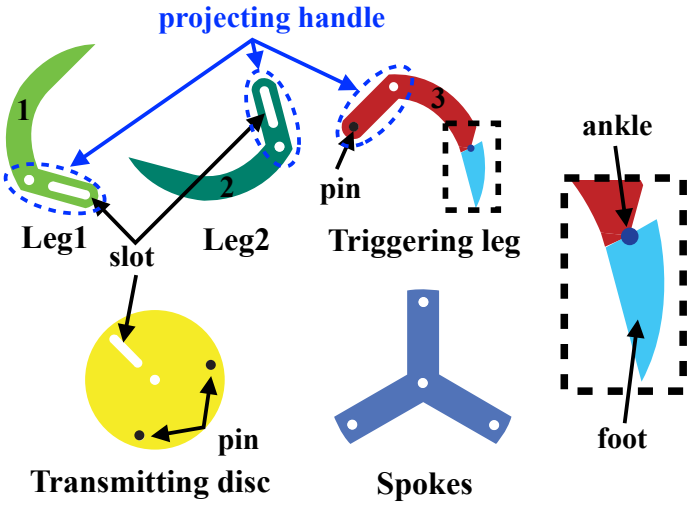

(a)

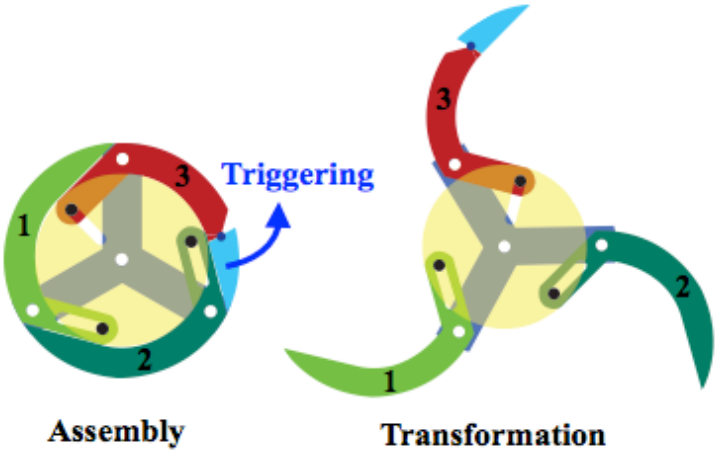

(b)

Fig. 2. Features of the passive transformable wheel: (a) Five components. (b) Assembly and Transformation.

2.2 Transformation mechanism

For the simplification of its design, the passive transformable wheel must utilize only the friction with an obstacle, not an actuator. However, we cannot expect a constant friction force, since it would vary with the type and condition of the terrain. Therefore, in order to raise the success rate of transformation, the wheel must take advantage of low frictions.

The initial development of the passive transformable wheel included three pins, each of which was located at the projecting handle of each leg, and all three slots were located symmetrically on the transmitting disc, 120° apart from one another. As a result, when torque was applied to one leg and even increased, the other two could not rotate. However, when the three pins and slots were asymmetrically located on the transmitting disc and three legs, the transformation easily occurred by the triggering leg's rotation.

Fig. 3(a) shows the pin-slider linkage system in which the three legs are connected to the transmitting disc by pins and slots. Fig. 3(b) and (c) show the mechanisms of the pin rotating the slot, and the slot rotating the pin, respectively. In Fig. 3, the arrow with the solid line represents the direction of the force, and the dashed line indicates the direction of the pin's or slot's movement. As seen in Fig. 3(b), in the rotating slot mechanism, the initial angle between the pin's moment arm

and the slot's moment arm is perpendicular, allowing the pin to slide smoothly along the slot. As the pin moves up the slot, the angle between the solid and the dashed arrows becomes smaller than 90°, so a portion of the torque acted upon the pin becomes the torque directing the slot's movement. Thus, the rotation of the pin generates the rotation of the slot. In the case of the rotating pin mechanism, the force on the slot is perpendicular to the direction in which the pin is allowed to move, preventing the pin's rotation (Fig. 3(c)). Results of a RecurDyn simulation of the force required to unfold all three legs of the passive transformable wheel based on these two mechanisms are shown in Fig. 4 [16]. While the initial development requires a triggering torque of 120 Nmm, the modified version that used only the rotating slot mechanism requires 20 Nmm, a merely one sixth of the former. Therefore, the passive transformable wheel adopted the rotating slot mechanism in each of the three pin-slider linkage systems, allowing for a low triggering torque.

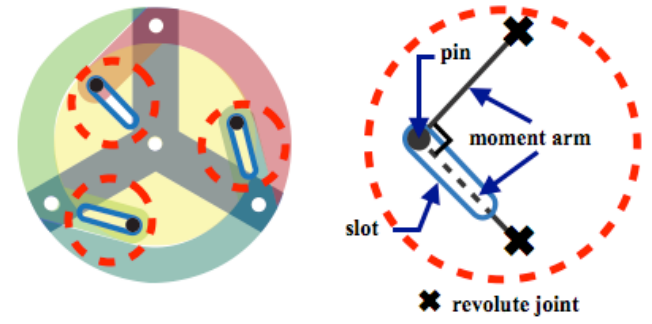

(a)

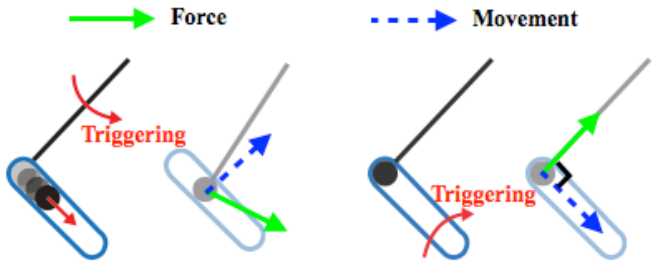

(b) (c)

Fig. 3. Asymmetrically arranged pins and slots in the passive transformable wheel: (a) Three pin-slider linkage systems at the joint between each leg and the transmitting disc. (b) The mechanism of the pin rotating the slot. (c) The mechanism of the slot rotating the pin.

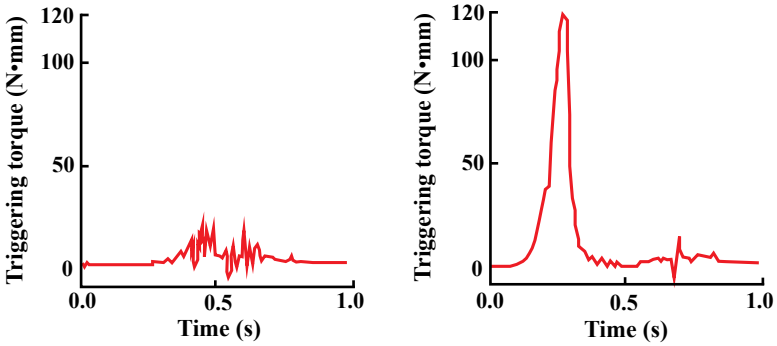

(a) (b)

Fig. 4. Simulation results of required triggering torque in two types of wheels: (a) The wheel uses only the mechanism of the pin rotating the slot with asymmetrical arrangement of pins and slots. (b) The wheel uses one mechanism of the pin rotating the slot and two mechanisms of the slot rotating the pin with symmetrical arrangement of pins and slots.

2.3 Triggering mechanism

The success of transformation from circular wheels into legged wheels depends on the treading point of the triggering leg. When the triggering leg treads the surface near the corner of an obstacle, the transformation easily occurs. Fig. 5 illustrates how the use of an ankle enables it in comparison with the passive transformable wheel without an ankle. Fig. 5(a) shows when the transformable wheel encounters an obstacle without an ankle, and Fig. 5(b) represents the free body diagram (FBD) when the triggering leg—indicated as the leg 3—treads the surface below the center of mass. We assume that the wheel slowly rotates enough to be regarded as a quasi-static system. The triggering torque at the revolute joint of the

triggering leg, T_1, is expressed as

$$T_1 = F_N d_1 + F_f h_1 + \mu F_f d_2 - F_f h_2 \,. \tag{1}$$

F_f is the friction force at the treading point, which is identical with reaction force at the contact point between the triggering leg and wall of an obstacle. F_N is the normal force at the treading point. The vertical distance between the revolute joint of the triggering leg and the treading point is represented as h_1. The horizontal distance 'from' the revolute joint 'to' the treading point is named as pivot distance, which is indicated as d_1. The vertical and horizontal distances between the revolute joint of the triggering leg and the contact point of the triggering leg with wall of an obstacle are also indicated as h_2 and d_2, respectively. Friction coefficient is expressed as μ. As the wheel continues to rotate, d_2 and h_2 reach to 0; thus, (1) can be restated as

$$T_1 = F_N d_1 + F_f h_1 \,. \tag{2}$$

The normal force at the treading point is the same as the weight of the robot, and it hinders the process of transformation because the sign of pivot distance is negative. Even if F_f increases T_1, the transformation hardly occurs because the weight of the

robot is much greater than the friction force.

Fig. 5(c) shows how the use of an ankle enables the triggering leg to tread at the corner of an obstacle. As seen in Fig. 5(c), the friction force between the foot and an obstacle rotates the foot in the counterclockwise direction with respect to the ankle joint. The foot protrudes from the circumference of the wheel, and as the wheel continues to rotate, the foot approaches the corner of an obstacle and is planted. Fig. 5(d) illustrates the FBD of the whole system, and it consists of FBDs of the triggering leg (Fig. 5(e)) and the leg 2 (Fig. 5(f)). As shown in Fig. 5(e), the triggering torque, T_1, is generated at the revolute joint of the triggering leg due to F_N.

$$T_1 = F_N d_1 - F_f h_1 \tag{3}$$

Like the case of the passive transformable wheel without an ankle, F_f is far smaller than F_N. T_1 generates the torque opening the leg 2, T_2, at the revolute joint of the leg 2 via the torque at the transmitting disc, T_0. The relation between T_1 and T_2 will be expressed in Section 3. In Fig. 5(f), the condition for the occurrence of transformation is represented as

$$T_3 - F_{N2} d_3 + F_f h_3 \geq 0 \tag{4}$$

where d_3 and h_3 are horizontal and vertical distances between the revolute joint of the leg 2 and the contact point, respectively. Even though F_{N2} hinders the transformation, d_3 reaches to 0 as wheel rotates; thus, the transformation occurs.

Since the friction forces are much smaller than the normal forces in (2) and (3), the pivot distance dominates the triggering torques in both cases. Therefore, the passive transformable wheel takes advantage of normal force at treading point for its transformation with an ankle, converting the sign of pivot distance from negative to positive.

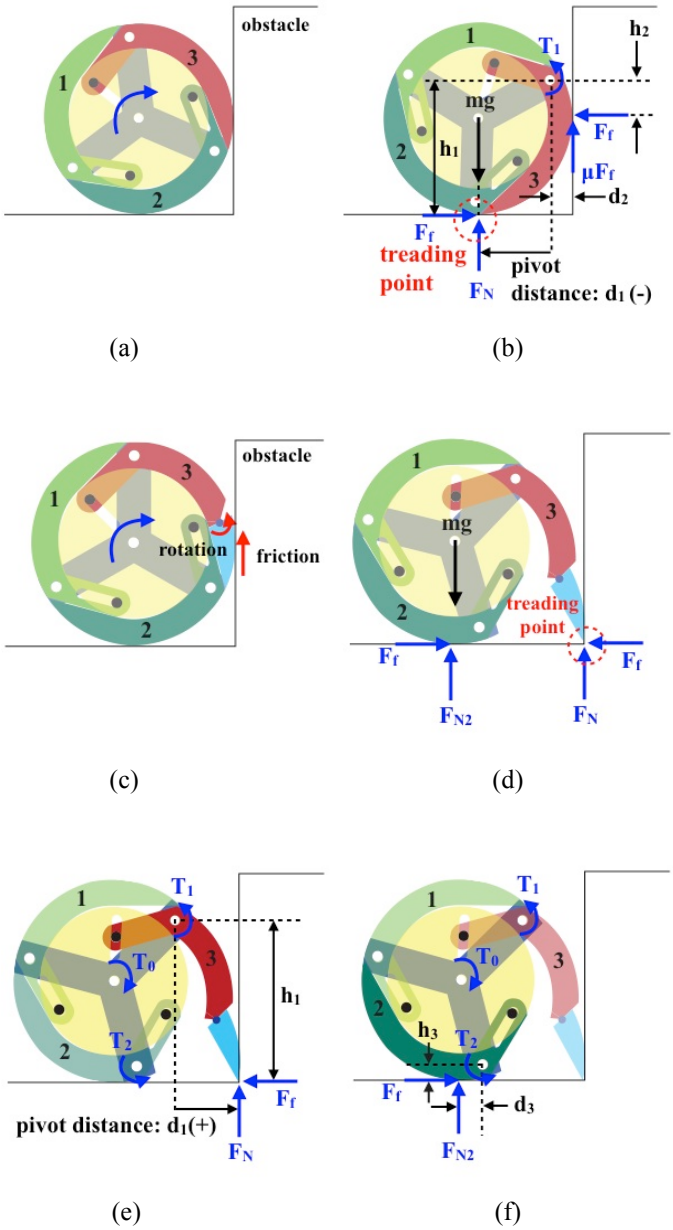

Fig. 5. Schematic diagrams of the triggering mechanism with an ankle: (a) The transformable wheel encounters an obstacle without an ankle. (b) The FBD of the triggering leg without an ankle. (c) The foot rotates due to the friction. (d) The foot treads at the corner of an obstacle. (e) The FBD of the triggering leg with the ankle. (f) The FBD of the leg 2.

2.4 Climbing scenario

When the transformation is initiated by the frictional force generated by the contact between the wheel and the wall of an obstacle, the passive transformable wheel can climb over an obstacle taller than the radius of its circular form. Fig. 6 illustrates the transformable wheel's scenario of climbing over an obstacle. In Step 1, the frictional force with the obstacle's wall protrudes the triggering leg's foot from its circumference, forming a point of support on the ground at the corner of an obstacle. In Step 2, as the motor continues to revolve, the wheel rotates while the supporting point is fixed, and the transformation into the legged wheel is completed. In Step 3, then the leg 1, following the triggering leg, treads on the upper surface of the obstacle. This treading point here then becomes the axis of the robot's rotation, and the wheel climbs over an obstacle by rotating about the treading point. In Step 4, the robot's weight forces the wheel to fold back when the triggering leg is directly below the center of the wheel.

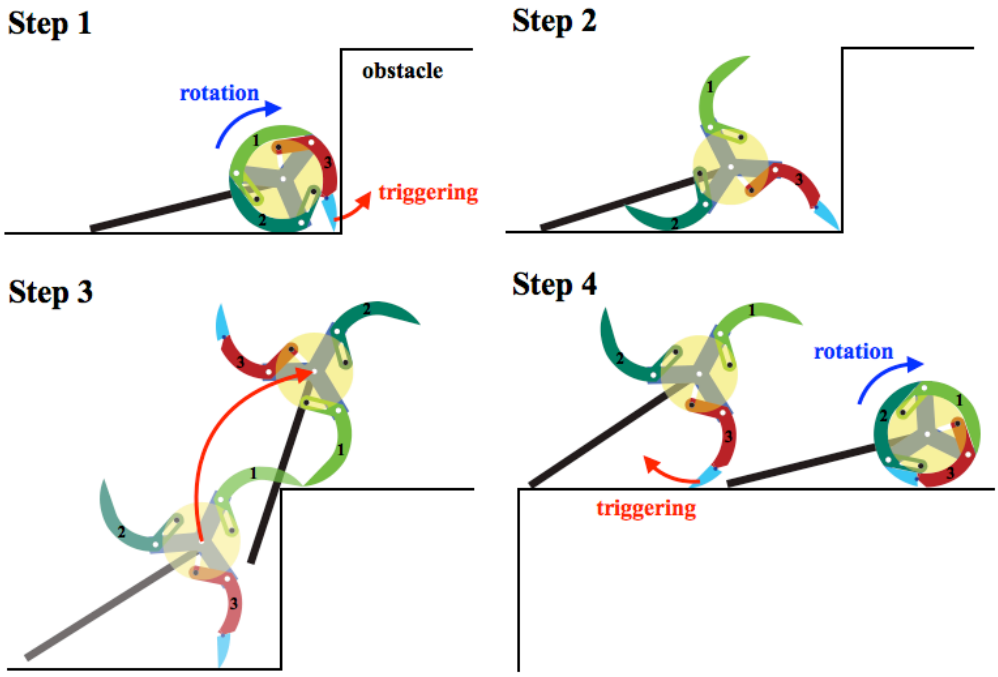

Fig. 6. Schematic diagrams of the climbing scenario. Through this scenario, the maximum height of the obstacle that the passive transformable wheel can climb over is taller than wheel's radius.

3. Design optimization

The initially designed the passive transformable wheel was tuned for its better climbing ability and higher success rate of the transformation. With the optimization of its design parameters, the wheel could raise the height of an obstacle it can climb over up to maximum. Moreover, this process did not affect the triggering torque required for the transformation, maintaining it at the same level. The geometry of the foot was also optimized, so the transformation occurred with 100% success rate in all wheel's angular velocity.

3.1 Modeling of the passive transformable wheel

The quasi-static model of the passive transformable wheel should be derived before tuning the design parameters because the triggering torque necessary for the transformation should not be raised in all optimization processes. For this purpose, we analyzed the ratio of T_2 to T_1, which is named as the wheel efficiency.

Fig. 7 shows the circular form of the passive transformable wheel before the transformation and an arbitrary state during the transformation. In an enlargement of part 'A,' the coordinates of the pin *(x, y)* can be expressed as

$$(x, y) = (-r\cos(\alpha)\sin(\theta), r - r\cos(\alpha)\cos(\theta)) \tag{5}$$

where θ and r are the angular displacement of the triggering leg and the radius of wheel before the transformation, respectively. Alpha is the design parameter, which is initial value of θ. The directions of the slot's movement and the force on the pin are labeled with a dashed arrow and solid arrow, respectively. The tangent value of the angle between the two arrows, a and b, is

$$\tan(a + \pi - b) = \frac{\cos(\alpha)\sin(2\theta) - \sin(\theta)}{\cos(\theta) - \cos(\alpha)\cos(2\theta)} \tag{6}$$

, and the relationship of T_1 and T_0 can be expressed as

$$T_0 = T_1 \frac{l_s 1}{l_p 1} \frac{1}{\sqrt{1 + (\frac{\cos(\alpha)\sin(2\theta) - \sin(\theta)}{\cos(\theta) - \cos(\alpha)\cos(2\theta)})^2}} \tag{7}$$

where l_s and l_p are the moment arms of the slot and pin, respectively. An identical processes on the pin-slider linkage system between the transmitting disc and the leg 2 yields

$$\frac{T_2}{T_1} = \frac{1}{2}\frac{l_s1}{l_p1}\frac{l_s2}{l_p2}\frac{1}{\sqrt{(1+(\frac{\cos(\alpha)\sin(2\theta)-\sin(\theta)}{\cos(\theta)-\cos(\alpha)\cos(2\theta)})^2)(1+(\frac{\sin(\alpha)\sin(2\delta)-\sin(\delta)}{\cos(\delta)-\sin(\alpha)\cos(2\delta)})^2)}} \quad (8)$$

where δ is the angular displacement of the transmitting disc. Again, in Fig. 5, l_p1 can be expressed as

$$l_p1 = r\cos(\alpha) \ . \quad (9)$$

Using the Second Law of Cosines on the triangle with sides of l_p1, l_p2, and r, l_s1 can be expressed as

$$l_s1 = r\sqrt{\cos^2(\alpha)+1-2\cos(\alpha)\cos(\theta)} \ . \quad (10)$$

With the same process on the transmitting disc and the leg 2's pin-slider linkage system, following equation can be derived.

$$\frac{l_s1}{l_p1}\frac{l_s2}{l_p2} = \frac{\sqrt{(\cos^2(\alpha)+1-2\cos(\alpha)\cos(\theta))(\sin^2(\alpha)+1-2\sin(\alpha)\cos(\delta))}}{\cos(\alpha)\sin(\alpha)} \quad (11)$$

Using the Second Law of Cosines on the triangle formed by l_p1, l_s1, and r, in Fig. 5,

cos(δ) can be expressed as

$$\cos(\delta) = \frac{l_s 1^2 + r^2 - l_p 1^2}{2 r l_s 1} \quad (12)$$

Substituting (9) and (10) in (12) with yields

$$\cos(\delta) = \frac{1 - \cos(\alpha)\cos(\theta)}{\sqrt{\cos^2(\alpha) + 1 - 2\cos(\alpha)\cos(\theta)}} \quad (13)$$

Using (13) and (11), (8) is expressed in terms of α and θ. The simulation result of the wheel efficiency is shown in Fig. 8.

As seen in Fig. 8, the wheel efficiency is minimized when the angular displacement of triggering leg, θ, is in the middle of the transformation phase. This result has a trend identical to that of RecurDyn simulation [16]; the middle phase of transformation requires the greatest torque. This minimum value is nearly constant in all values of α.

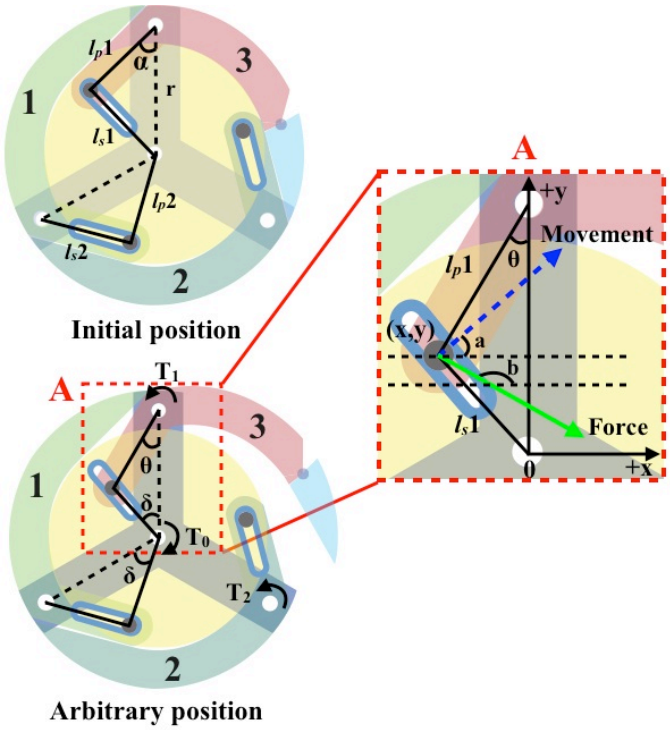

Fig. 7. Variables and parameters used to model the efficiency of the passive transformable wheel.

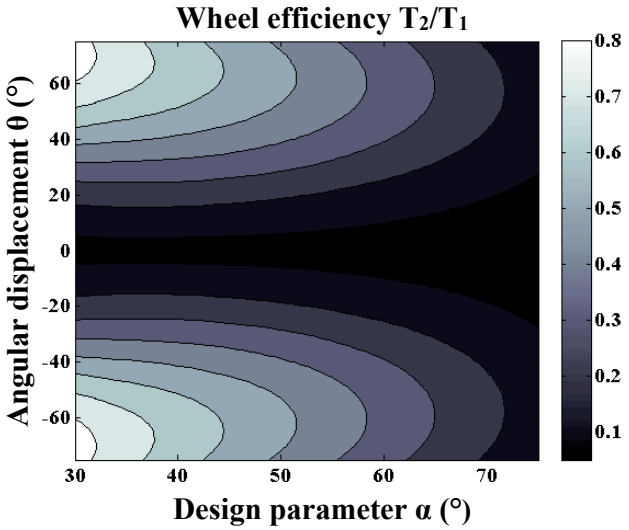

Fig. 8. The efficiency of the passive transformable wheel. The minimum wheel efficiency (at θ = 0°) stays constant regardless of the value of the design parameter α.

3.2 Maximizing the transformation ratio

The maximum height of an obstacle the wheel can climb over is affected by the transformation ratio, which is the ratio between the radii before and after the transformation. In Fig. 9(a), a geometric interpretation of the transformation ratio leads to

$$\frac{R}{r} = \sqrt{4 - 2\sqrt{3}\cos(2\alpha + \frac{\pi}{6})} \tag{14}$$

where R is the distance between the center of the wheel and the end of each leg in the legged wheel. As shown in (14), the transformation ratio totally depends on α, and it reaches its maximum when α=75°.

Another variable to be considered for the transformation ratio is the wheel efficiency. As shown in Fig. 8, the minimum value of the wheel efficiency is constant in all values of α; thus, increasing α to maximize the transformation ratio has minimal effect on the overall efficiency of the wheel. Because the transformation ratio is nearly independent from wheel efficiency, the design parameter α should increase up to 75° as possible to maximize the transformation ratio.

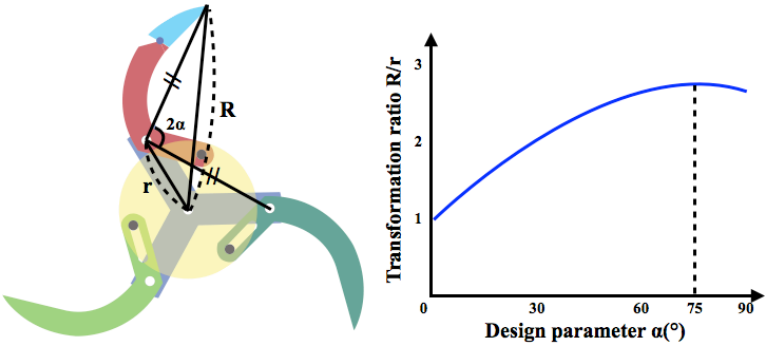

Fig. 9. The transformation ratio indicated as the ratio between radii before and after the transformation. It reaches its maximum when α=75°.

3.3 Foot design for the higher success rate of the transformation

Since the minimum wheel efficiency is independent with α, it is hard to increase the T_2 by tuning the parameters in this modeling; thus, we aimed to increase the input triggering torque, T_1, by foot design optimization.

As mentioned in Section 2, if the treading point of the triggering leg is placed at the corner of an obstacle, the transformation easily occurs. In Fig. 10(a), the length that allows the foot to do so is geometrically analyzed, and it can be found from the following condition.

$$L_f \sin(\beta) \geq (\sqrt{2}-1)r + \frac{t}{2} \tag{15}$$

L_f is the length of the foot, β is the angular displacement of the foot's rotation, and t is the thickness of the leg. As expressed in (3), if the pivot distance increases, the triggering torque on the joint, T_1, does as well, enabling the wheel to be transformed. From (15), the chosen values were L_f=23.5 mm and β=60° while r=40 mm and t=8 mm. The efficacy of the ankle was tested at least three times at the vertically raised platform as shown as Fig. 10(a). Fig. 10(b) shows the relationship between the pivot distance and the angular velocity of the wheel with and without the ankle. As expected, the pivot distance increased when the wheel has the ankle. With this tuned ankle, the legs unfolded upon the contact with the obstacle regardless of its angular velocity. Without the ankle, however, the wheel was unable to transform with angular velocities of 1-3 rad/s. For angular velocities of 4, 5, 6, and 7 rad/s, the success rate of transformation was 50, 67, 75, and 75% respectively, and 100% for 8 rad/s and up. As the angular velocity increases, the motor's torque increases as well, raising the normal force of the triggering leg acting upon the obstacle's wall. By the increased friction force between them, the triggering leg rotated on its revolute joint and trod on the ground near the obstacle. In this case, however, the robot cannot stably climb over the obstacle due to excessive repulsive forces from the impact of the rotating legs on the ground. Therefore, an ankle must be used to facilitate the transformation even at low speeds.

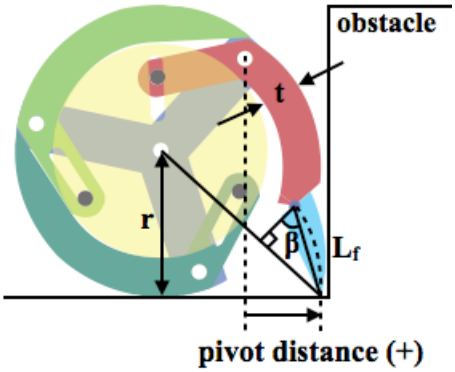

(a)

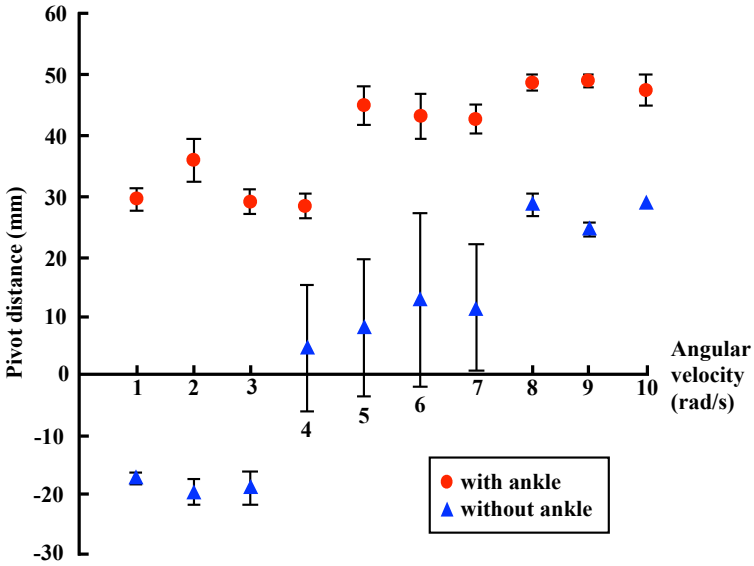

(b)

Fig. 10. The design optimization of foot to increase the pivot distance: (a) The parameters for foot design. (b) The pivot distance with and without the ankle. With the ankle, the pivot distance is almost above 30 mm, which is sufficient to transform the circular wheel into the legged wheel regardless of the wheel's angular velocity.

4. Design of the robotic platform

A simple robotic platform, Wheel Transformer, was fabricated to verify the performance of the new kind of transformable wheel (Fig. 1 and 11). For stable obstacle climbing, the body length and motor's angular velocity were tuned to reduce the slip at contact point between the ends of legs and the obstacle.

4.1 Features

Some previously developed robots were able to climb over obstacles taller than the radius of their wheels with linkage systems or the propulsion of the rear wheels [17]-[21]. However, to test the obstacle climbing ability of just the passive transformable wheel, these additional advantages must be excluded. Thus, Wheel Transformer used only the two transformable wheels. In order to minimize energy loss that might be caused by transmission systems, each wheel was attached directly to the motor's axis. Steering was made possible by independently rotating both wheels (differential steering).

In terms of electronics, one servo controller for each of the two motors was used in this robot. When the DC motors are controlled by pulse width modulation (PWM), they require a lower voltage input for lower speeds, resulting in a lower

torque. In the process of climbing an obstacle, the robot needs slow motor revolutions to reduce repulsive forces from the collision of the legs with an obstacle, but it also demands a high torque that can lift the robot's mass over an obstacle. The servo controller allows the motor to output a low speed but high torque. The main controller uses the XBee module to communicate wirelessly with the computer, and controls the servo controller with digital signals.

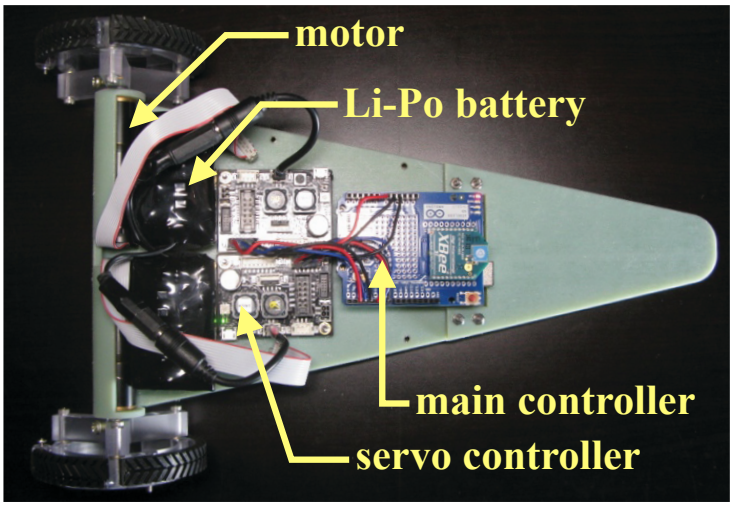

Fig. 11. The feature of Wheel Transformer.

4.2 Tuning design parameters for stable climbing

For the robot to climb over an obstacle, the stepping leg must be the center of rotation, without slipping. Fig. 12 is the FBD of Wheel Transformer climbing a raised platform. The greater the normal force at this point $F1_y$ is, the more stable the robot can climb over the obstacle. In Fig. 12, the movement of the coordinates *(x, y)*

can be seen as a circular motion whose center is at the end of the leg and radius *R*. The angular speed is constant due to the servo controllers. Thus, the kinematic equations of the coordinates *(x, y)* are

$$F1_x = -mR\omega^2 \cos(\psi) \tag{16}$$

$$F1_y + F2_y - mg = -mR\omega^2 \sin(\psi) \tag{17}$$

$$F1_x R\sin(\psi) - F1_y R\cos(\psi) + F2_y \sqrt{L^2 - (h + R\sin(\psi))^2} = 0 \tag{18}$$

where, F_x, F_y, L, ω, and ψ indicate the horizontal and vertical reaction forces, the length of the robot's body, the angular velocity of the wheel, and the angular displacement of the stepping leg, respectively. Substituting (16) and (17) into (18) yields $F1_y$ as a following equation.

$$F1_y = \frac{m(g - R\omega^2 \sin(\psi) - \frac{R^2\omega^2 \sin(\psi)\cos(\psi)}{\sqrt{L^2 - (h + R\sin(\psi))^2}})}{1 + \frac{R\cos(\psi)}{\sqrt{L^2 - (h + R\sin(\psi))^2}}} \tag{19}$$

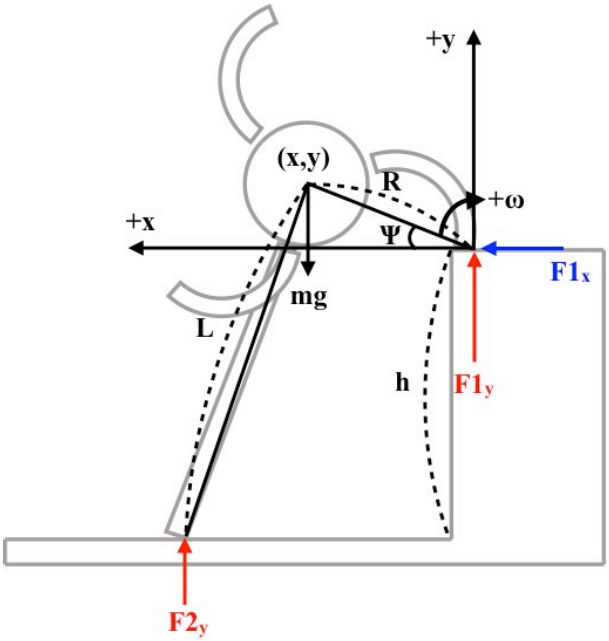

Fig. 12. The FBD of Wheel Transformer climbing a raised platform.

The simulation was run for h of 130 mm, m of 0.7 kg, and R of 85 mm, with L and ω as the design parameters. Fig. 13(a) represents $F1_y$ with respect to changes in L and ψ at ω=1 rad/s. As L increases, the normal force also increases, allowing the robot to stably climb over the obstacle. The reason for this is that as L increases, $F2_y$ becomes farther away from the center of mass, increasing the portion of weight that $F1_y$ supports. Fig. 13(b) represents $F1_y$ with respect to changes in ω and ψ at L=0.3 m. When the value of ψ varies from -30° to 90°, as ω increases, the normal force decreases, because as the velocity of the leg stepping on the top surface of the obstacle increases, the repulsive force increases upon impact. Empirically, Wheel

Transformer was able to stably overcome the raised platform with a height of 130 mm without slipping at L values of 0.3 m or greater, and ω values of 1 rad/s or smaller. $F1_y$ values at L=0.3 m and ω=1 rad/s were respectively shown as the cross section labeled 'A' in Fig. 13(a) and (b), and these values are shown in a 2-dimensional plot with a dotted line in Fig. 13(c). The solid line represents experimental values using a load cell (capacity: 1 kgf, resolution: 0.05 gf, CASKOREA Corp.), and approximates to values obtained in simulation results. Errors are caused by the difference between the assumption and real situation; the slight off-centeredness of the robot's center of mass from the wheel's center. Combined with results from Fig. 10, it was found that both the easy transformation and the stable climbing were possible at ω=1 rad/s.

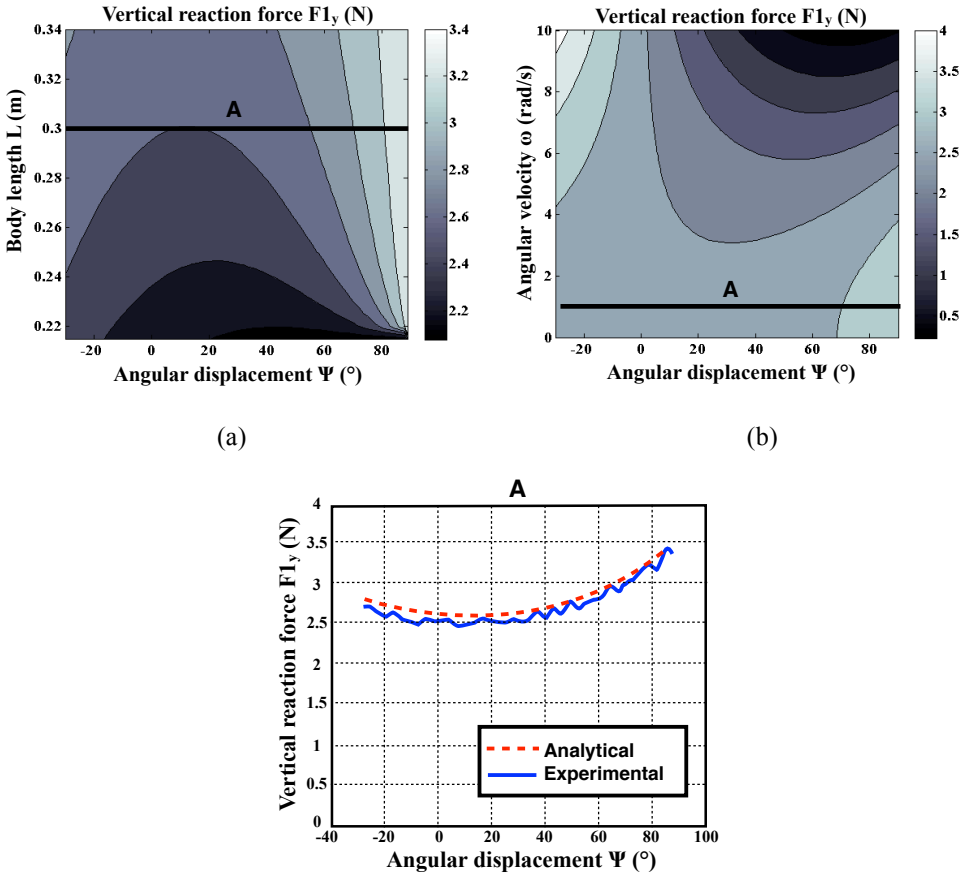

Fig. 13. Analytical and experimental results of normal force as a function of rotational angle of leg (ψ): (a) Body length (L) at ω=1 rad/s is the design parameter. (b) Angular velocity of motor (ω) at L=0.3 m is the design parameter. (c) Two-dimensional graph of intercept A in (a) and (b).

5. Results

The new kind of transformable wheel and Wheel Transformer were fabricated based on the analyses in Section 2, 3, and 4 (Fig. 1). The physical specifications are elaborated in Table I. The passive transformable wheel and Wheel transformer was created by a CNC milling machine and a 3D printer, respectively.

TABLE I

PHYSICAL SPECIFICATIONS OF THE PASSIVE TRANSFORMABLE WHEEL & WHEEL TRANSFORMER

Passive Transformable Wheel	
Circular wheel radius	40 mm
Legged wheel radius	85 mm
Transformation ratio	212.5 %
Max. obstacle height	150 mm
Weight	63 g
Material	polycarbonate & rubber pad (Misumi Corp.)
Wheel Transformer	
Size	210 x 340 x 80 (width x length x height)
Weight	700 g
Motors	Maxon DC motor (4.5W; 16 mm dia.) x2 Rated voltage : 12V Rated torque : 4.26 mNm Rated current : 0.569 A Max. speed : 16000 rpm
Gearheads	Maxon 84:1 planetary gearhead x2
Encoders	Maxon 512 CPT encoder x2
Servo controllers	Escon 36/2 DC servo controller x2
Main controller	Arduino Uno R3 with Xbee module
Batteries	Li-Po battery x2 (14.8V, 1400 mAh per pack)

The passive transformable wheel incorporates the functional advantages of both circular wheels and legged wheels. To be specific, when the wheel maintains its circular shape, the robot can display its stable and efficient driving performance on flat surfaces without any oscillations of its center of the mass. When the wheel transforms into the legged wheel, on the other hand, it obtains the ability to climb over obstacles taller than the wheel radius. In this section, we evaluate the performance of each mode.

5.1 Speed & specific resistance

In the typical circular-wheel mode, the distance between the center of the wheel and the point of contact with the ground stays constant as wheel's radius, which makes it possible for the robot to move stably and efficiently without any vertical oscillations. When the robot maintains stable contact with the ground, it continuously gains propulsion and its driving speed increases. Accordingly, the speed of the robot is proportional to its driving stability. The efficiency of the robot is evaluated by its specific resistance S [22].

$$S = \frac{P(v)}{mgv} \tag{20}$$

P(v) and *v* refer to the total power consumption rate of the battery and the speed of the robot, respectively. Fig. 14(a), (b), and (c) denote the specific resistance on flat surfaces, pitch angles of the robot, and the electric current consumption of the motor in the circular-wheel mode and the legged-wheel modes. These lead us to the following three conclusions:

1) In the circular-wheel mode, the robot's speed reached its maximum, 0.8 m/s (2.4 body lengths per second, the upper limit value of the motor's capacity). With the legged wheels, however, it did not exceed 0.3m/s (0.9 body length per second) (Fig. 14(a)). Increasing the rpm of the motor (arrows in Fig. 14(a)) consequentially increases the repulsive force generated when the leg hits the ground. As the robot bounces, the normal force decreases. Thus, in the legged-wheel mode, the robot cannot gain any more speed due to the resultant decrease in friction. When the motor rotated at 60 rpm, the speed of the robot was 0.3 m/s and specific resistance is 4.66. When the motor, however, rotated at 80 rpm, the speed of the robot was 0.15 m/s and specific resistance is 10.44, and the robot was unable to drive faster even at motor rotated over 80 rpm.
2) Since the center of robot's mass oscillates vertically, legged wheels have markedly greater specific resistance (Fig. 14(a)). As shown in Fig. 14(b),

pitch angles of the robot in the legged-wheel mode were plotted on a sinusoidal curve with a constant amplitude and period, whereas pitch angles of the robot in the circular-wheel mode stayed almost constant. These results suggest that the center of the robot's mass moved upward and downward as motor rotated since the radius of wheel's rotation was not retained as same value. Therefore more electric current was consumed when the center of the robot's mass moved upward and it is indicated in Fig. 14(c). The mean current consumption is 0.3 A in the legged-wheel mode, which is significantly higher than 0.07 A in the circular-wheel mode at the same motor input (10 rpm). Mini Whegs and RHex, with four and six legged wheels, lower energy consumption by decreasing the amplitude of the center of mass displacement curve with a diagonal walking gait and a tripod walking gait, respectively [4][5]. Wheel Transformer, however, demonstrates relatively high energy consumption in legged-wheel mode with only the two transformable wheels.

3) Depicted on an inverse proportion curve in Fig. 14(a), the specific resistance decreases as the speed increases in the circular-wheel mode because the speed increases at a higher rate than the power consumption does. The specific resistance is 0.7 at 0.8 m/s in the circular-wheel mode, which is comparable

to the specific resistance of previously developed robots at the same speed (Roller-Walker: 0.7 [23], Scout II: 1.4 [24], iSprwal 2.0: [25], RHex 4.0: [26]).

Specific resistance varies depending on whether the electric current is consumed solely by the motors or by the entire robot [23]. Most robots incorporating the wheel-leg hybrid locomotion adopt additional actuators for switching modes along with the essential actuators for the robot's locomotion, varying specific resistance. On the contrary, Wheel Transformer has only two motors to operate the passive transformable wheels, with no additional actuator. The current consumption of the actuators is almost equal to that of the entire robot. Consequently, replacing the motor with a more efficient one can lower specific resistance.

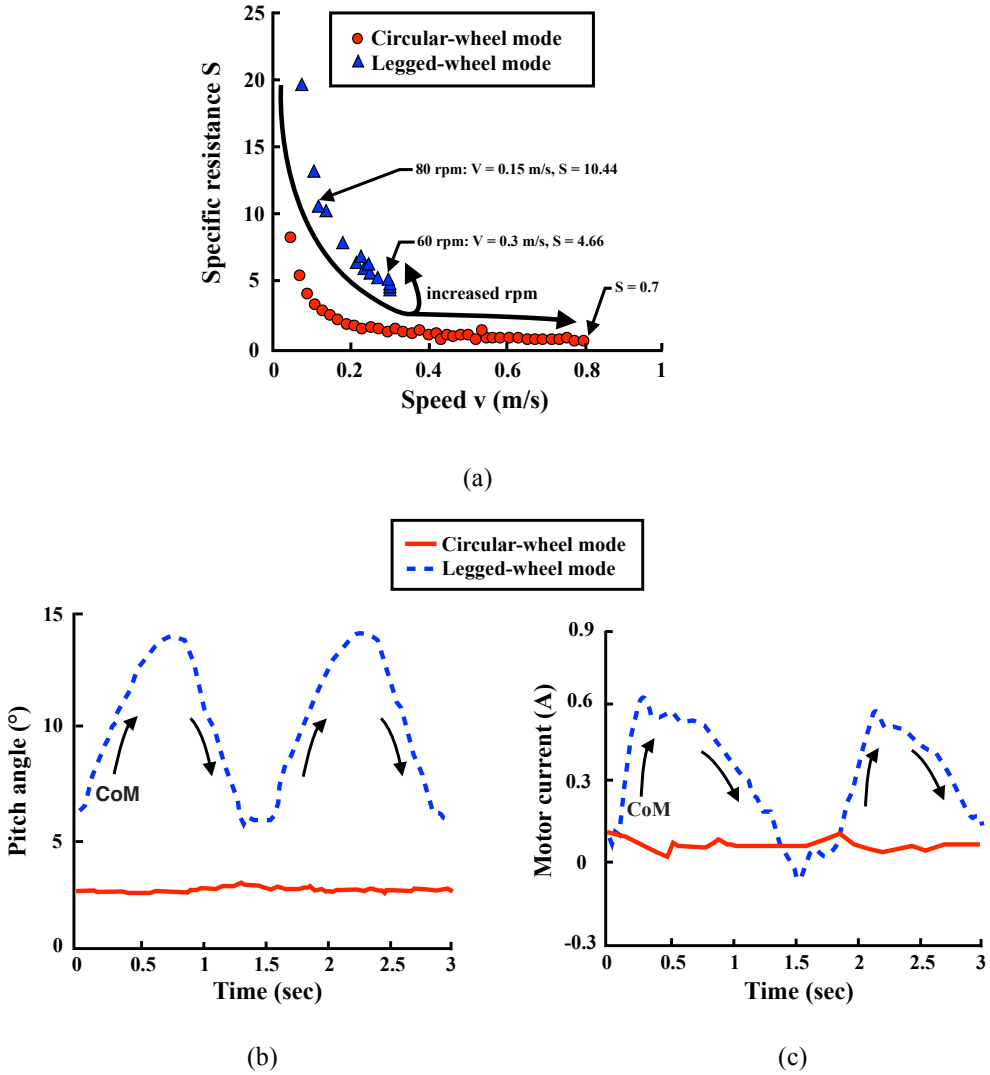

Fig. 14. The performance evaluation for the circular-wheel mode: (a) The specific resistance. (b) The pitch angles of the robot. (c) The electric current consumptions of each motor.

5.2 Obstacle climbing

The improved climbing ability in the legged-wheel mode is evidenced by Fig. 15(a) and (b), which show that the robot can climb a raised platform and a staircase unclimbable in the circular-wheel mode. The angular velocity was set at 1 rad/s to ease the transformation process and minimize the slip of the legs during climbing as studied in section 3 and 4.

The obstacle in Fig. 15(a) is a 130mm-tall raised platform, which is 3.25 times as tall as the circular wheel's radius. The body of Wheel Transformer was designed to easily climb over a 130 mm-tall obstacle with a 100% success rate. With taller obstacles, however, the legs kept slipping and were not able to heave up the center of mass over the edge of the obstacle. On the other hand, the legged wheel could place its leg on the top of platforms as tall as 150mm. When only one of the triggering legs came in contact with the obstacle and the legged wheel placed its leg on the top surface before the other one did, the robot body was laterally tilted, making it impossible for the other legged wheel to place its leg on the obstacle. This problem stems from the phase difference between the two triggering legs, which calls for further research on the phase sensing.

Fig. 15(b) shows Wheel Transformer climbing a staircase with a height of 100 mm. Quattroped with four legged wheels and RHex and Whegs with six legged

wheels are able to climb stairs without slipping by means of propulsion from their rear wheels [14][4][6]. Although Wheel Transformer has less propulsion with only two legged wheels [27], it has the merit of not needing to control the phase between the front and rear wheels.

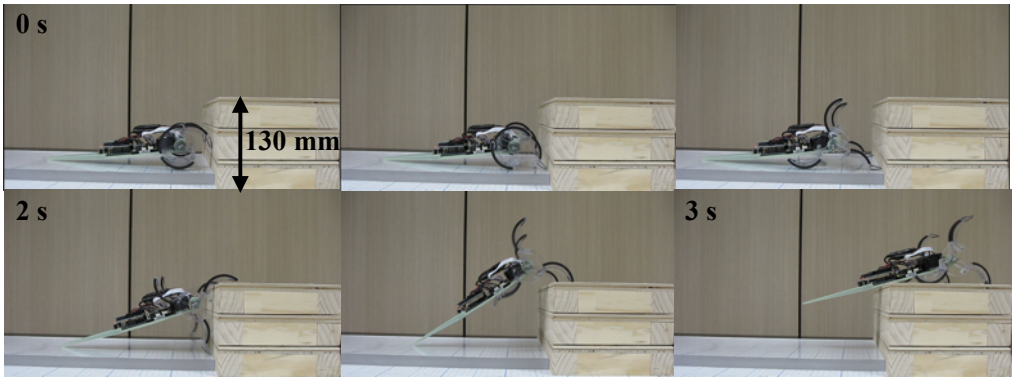

(a)

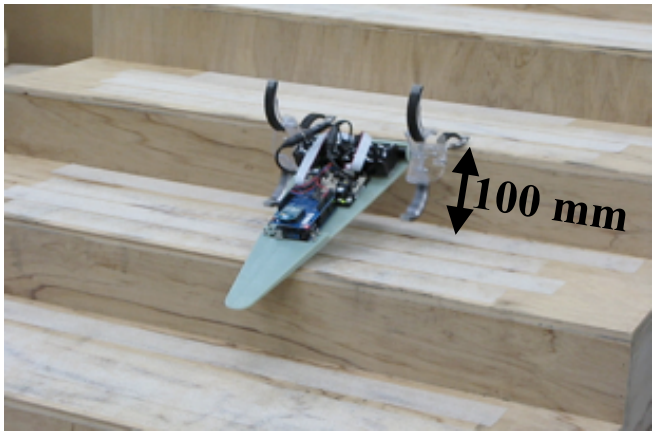

(b)

Fig. 15. Scenes of the robot climbing the obstacles: (a) The raised platform. (b) The staircase.

5.3 Discussion about mode switch

For the passive transformable wheel's legs to unfold using only the frictional force caused by contact with an obstacle, the wheel must rotate toward the wall so the foot makes contact with the wall before the triggering leg does. However, when the wheel rotates at high speeds on flat surfaces, the centrifugal force caused the legs to unfold; the legs unfolded when the wheel rotated over 4.2 rad/s. Moreover, they also unfolded when the foot was caught in small gaps on the ground. On the other hand, if the wheel rotated in the opposite direction, the wheel is unable to transform, due to the mechanism explained in Fig. 5(b); contact between the triggering leg and the ground always occurs below the center of the wheel, and the robot's mass hinders the transformation. Therefore, for high-speed locomotion, the wheel must rotate in the opposite direction. However, if the wheel rotates in the opposite direction without flipping the body over the wheels, the body will hinder the robot's locomotion being caught by rough terrain. Thus, the body must flip over when switching between the circular-wheel and legged-wheel modes.

Fig. 16 illustrates the principle of mode switch between the two modes using only 2 DC motors, which are already used for robot's locomotion. Fig. 16(a) shows the principle of switching from the legged-wheel mode to the circular-wheel mode. In Fig. 16(a), D_2 indicates the distance between the hind leg's stepping point

and the robot's center of mass, and D_1 indicates the distance between the center of the wheel and the robot's center of mass. If D_2 is greater than D_1, the torque required to back up the robot is greater than the torque required to flip the body over. Therefore, if the motor rotates backward, the wheel will stay and the body will flip over the wheels by the relative motion. In this mode switch, however, the hind leg must not be the triggering leg because D_2 will be zero when the triggering leg is folded. If the hind leg is one of the other two legs, then D_2 will be sustained because the other legs cannot be folded by the rotating pin mechanism (self-locking mechanism). Fig. 16(b) illustrates the switch from the circular-wheel mode to the legged-wheel mode using the same principle. The distance between the hind leg's stepping point and the robot's center of mass, D_3, is longer than D_1, so the body will flip over the wheels by the relative motion of the motor's backward rotation. In the circular-wheel mode, if the wheel rotates backward very quickly, it transforms into the legged wheel by centrifugal force, and the body flips over.

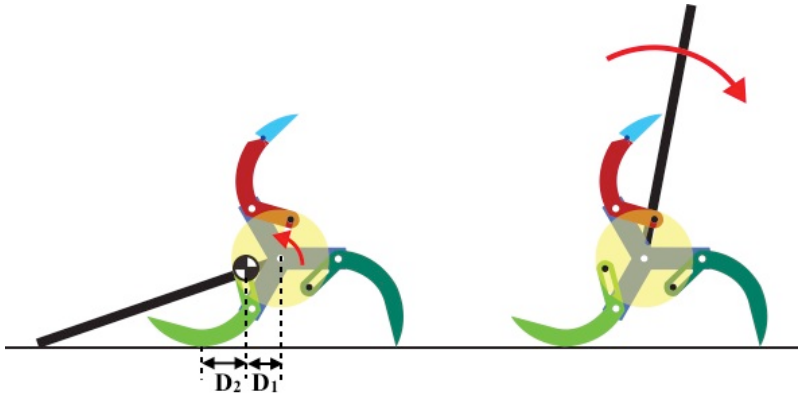

(a)

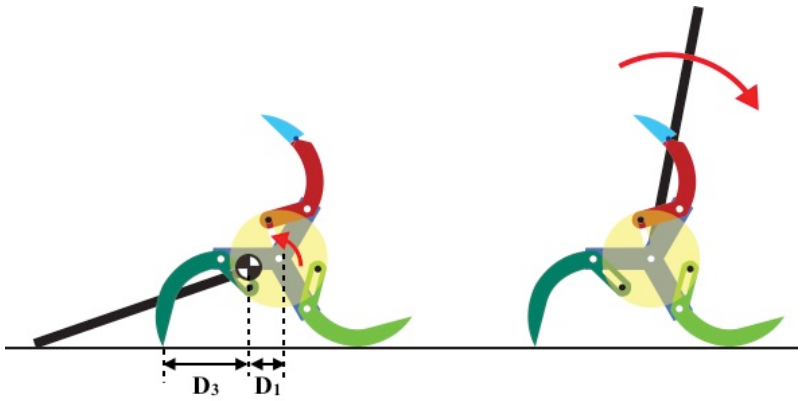

(b)

Fig. 16. Design for mode switch using relative motion: (a) Switching from the legged-wheel mode to the circular-wheel mode using self-locking mechanism. (b) Switching from the circular-wheel mode to the legged-wheel mode.

6. Conclusions

In this study, we developed the new kind of transformable wheel that has strengths of both circular wheels and legged wheels; stable and energy efficient driving ability of circular wheels and obstacle climbing ability of legged wheels. In Section 2, we designed the five components for the coupled-leg system of the passive transformable wheel. The ankle was used to ease the transformation into the legged wheel. In Section 3, we adjusted the design parameter α to maximize the transformation, maintaining low triggering torque. In Section 4, we discussed Wheel Transformer in terms of features and tuning of its design parameters for stable climbing. In Section 5, the performance was evaluated in both circular-wheel and legged-wheel modes.

Wheel Transformer introduced in this study achieved a speed of 2.4 body lengths per second with specific resistance of 0.7 and an ability to climb over the obstacle of 130 mm in height, which is 3.25 times as tall as its radius of circular shape. Since Wheel Transformer used just two DC motors for its locomotion, steering, and the transformation of the wheels, it can achieve a more agile locomotion and lower specific resistance by merely improving its motor capabilities. Future works in this study may include controlling the phases of the triggering legs while

climbing so that the transformation occurs simultaneously in both wheels, preventing the body from tilting laterally.

The passive transformable wheel was developed for small robotic systems that have an advantage in SAR missions. In other words, the robot's size may be freely reduced or expanded, due to the simplicity of its design, which allows transformation without additional actuators. In addition to this advantage, a compact design will simplify the control strategy and lower the manufacturing cost, allowing it to be easily applied to swarm robotic systems, which can maximize its mission success rate.

References

[1] D. F. Hougen, S. Benjaafar, J. C. Bonney, J. R. Budenske, M. Dvorak, M. Gini, H. French, D. G. Krantz, P. Y. Li, and F. Malver, "A miniature robotic system for reconnaissance and surveillance," in *Proc. IEEE Int. Conf. Robot. Autom.*, 2000, pp. 501-507.

[2] F. Matsuno, and S. Tadokoro, "Rescue robots and systems in Japan," in *Proc. IEEE Int. Conf. on Robotics and Biomimetics*, 2004, pp.12-20.

[3] M. Kaspari, and M. D. Weiser, "The size–grain hypothesis and interspecific scaling in ants," *Functional Ecology,* vol. 13, no. 4, pp. 530-538, 1999.

[4] R. D. Quinn, J. T. Offi, D. A. Kingsley, and R. E. Ritzmann, "Improved mobility through abstracted biological principles," in *Proc. IEEE/RSJ Int. Conf. Intell. Robots Syst.*, 2002, pp. 2652-2657.

[5] J. M. Morrey, B. Lambrecht, A. D. Horchler, R. E. Ritzmann, and R. D. Quinn, "Highly mobile and robust small quadruped robots," in *Proc. IEEE/RSJ Int. Conf. Intell. Robots Syst.*, 2003, pp. 82-87.

[6] U. Saranli, M. Buehler, and D. E. Koditschek, "RHex: A simple and highly mobile hexapod robot," *Int. J. Robot. Res.,* vol. 20, no. 7, pp. 616-631, Jul. 2001.

[7] J. B. Jeans, and D. Hong, "IMPASS: Intelligent mobility platform with active spoke system," in *Proc. IEEE Int. Conf. Robot. Autom.*, 2009, pp. 1605-1606.

[8] F. Michaud, D. Létourneau, M. Arsenault, Y. Bergeron, R. Cadrin, F. Gagnon, M.-A. Legault, M. Millette, J.-F. Paré, and M.-C. Tremblay, "Multi-modal locomotion robotic platform using leg-track-wheel articulations," *Autonomous Robots,* vol. 18, no. 2, pp. 137-156, 2005.

[9] S. Hirose, "Variable Constraint Mechanism and Its Application for Design of Mobile Robots," *Int. J. Robot. Res.,* vol. 19, no. 11, pp. 1126-1138, Nov. 2000.

[10] J. A. Smith, I. Sharf, and M. Trentini, "PAW: a hybrid wheeled-leg robot," in *Proc. IEEE Int. Conf. Robot. Autom.*, 2006, pp. 4043-4048.

[11] T. Okada, W. T. Botelho, and T. Shimizu, "Motion Analysis with Experimental Verification of the Hybrid Robot PEOPLER-II for Reversible Switch between Walk and Roll on Demand," *Int. J. Rob. Res.*, vol. 29, no. 9, pp. 1199-1221, Aug. 2010.

[12] C. C. Phipps, B. E. Shores, and M. A. Minor, “Design and quasi-static locomotion analysis of the rolling disk biped hybrid robot,” *IEEE Trans. Robot.*, vol. 24, no. 6, pp. 1302-1314, Dec. 2008.

[13] K. Tadakuma, R. Tadakuma, A. Maruyama, E. Rohmer, K. Nagatani, K. Yoshida, A. Ming, M. Shimojo, M. Higashimori, and M. Kaneko, "Mechanical design of the wheel-leg hybrid mobile robot to realize a large wheel diameter," in *Proc. IEEE/RSJ Int. Conf. Intell. Robots Syst.*, 2010, pp. 3358-3365.

[14] S. Y. Shen, C. H. Li, C. C. Cheng, J. C. Lu, S. F. Wang, and P. C. Lin, "Design of a leg-wheel hybrid mobile platform," in *Proc. IEEE/RSJ Int. Conf. Intell. Robots Syst.*, 2009, pp. 4682-4687.

[15] D. P. Stormont, "Autonomous rescue robot swarms for first responders," in *Proc. IEEE Int. Conf. Computational intelligence for Homeland Security and Personal Safety*, 2005, pp. 151-157.

[16] Y. S. Kim, G. P. Jung, H. Kim, K. J. Cho, and C. N. Chu, “Wheel Transformer: A miniaturized terrain adaptive robot with passively transformed wheels,” in *Proc. IEEE Int. Conf. Robot. Autom.*, 2013, pp. 5625-5630.

[17] C. Grand, F. Benamar, F. Plumet, and P. Bidaud, “Stability and traction optimization of a reconfigurable wheel-legged robot,” *Int. J. Rob. Res.,* vol. 23, no. 10-11, pp. 1041-1058, Oct.-Nov. 2004.

[18] P. S. Schenker, T. L. Huntsberger, P. Pirjanian, E. T. Baumgartner, and E. Tunstel, “Planetary rover developments supporting mars exploration, sample return and future human-robotic colonization,” *Autonomous Robots,* vol. 14, no. 2-3, pp. 103-126, 2003.

[19] S. D. Herbert, A. Drenner, and N. Papanikolopoulos, "Loper: A quadruped-hybrid stair climbing robot," in *Proc. IEEE Int. Conf. Robot. Autom.*, 2008, pp. 799-804.

[20] T. Estier, Y. Crausaz, B. Merminod, M. Lauria, R. Piguet, and R. Siegwart, “An innovative space rover with extended climbing abilities,” in *Proc. Space and Robotics, 2000*, pp. 333-339.

[21] G. Quaglia, D. Maffiodo, W. Franco, S. Appendino, and R. Oderio, “The Epi.q-1 Hybrid Mobile Robot,” *Int. J. Robot. Res.*, vol. 29, no. 1, pp. 81-91, Jan. 2010.

[22] T. Von Karman, and G. Gabrielli, “What price speed? Specific power required for propulsion of vehicles,” *Mechanical Engineering,* vol. 72, pp. 775-781, 1950.

[23] G. Endo and S. Hirose, “Study on Roller-Walker: Energy efficiency of Roller-walk,” in *Proc. IEEE Int. Conf. Robot. Autom.*, 2011, pp. 5050-5055.

[24] I. Poulakakis, “Modeling and Experiments of Untethered Quadrupedal Running with a Bounding Gait: The Scout II Robot,” *Int. J. Robot. Res.*, vol. 24, no. 4, pp. 239-256, Apr. 2005.

[25] S. Kim, “iSprawl: Design and Tuning for High-speed Autonomous Open-loop Running,” *Int. J. Rob. Res.*, vol. 25, no. 9, pp. 903-912, Sep. 2006.

[26] D. Campbell, and M. Buehler, “Preliminary bounding experiments in a dynamic hexapod,” *Experimental Robotics VIII*, pp. 612-621, 2003.

[27] S. C. Chen, K. J. Huang, C. H. Li, and P. C. Lin, "Trajectory planning for stair climbing in the leg-wheel hybrid mobile robot quattroped," in *Proc. IEEE Int. Conf. Robot. Autom.*, 2011, pp. 1229-1234.

국문초록

본 논문에서는 원형 바퀴와 다리가 달린 바퀴를 모두 사용할 수 있는 새로운 형태의 로봇이 개발되었다. 이 로봇은 이동 수단으로 새로운 종류의 변신 바퀴를 사용하여, 원형 바퀴와 다리가 달린 바퀴의 장점을 모두 지니고 있다. 로봇의 설계를 단순하게 하기 위하여, 이 새로운 종류의 변신 바퀴는 변신을 위하여 별도의 구동 장치를 사용하지 않고, 변신은 장애물과의 접촉으로 인하여 피동적으로 이루어진다. 이를 위하여 이 변신 바퀴는 새로운 변신 유발 장치를 포함하고 있다. 다리가 달린 바퀴일 때의 장애물을 넘는 능력을 극대화 시키기 위하여 변신 바퀴와 로봇의 설계 요소들이 역학적 분석을 통하여 최적화 되었다. 그리고 이 로봇의 성능은 주행 안전성, 에너지 효율, 로봇이 넘을 수 있는 최대 장애물 높이의 면에서 평가되었다. 이 새로운 종류의 변신 바퀴를 이용하여, 로봇은 원형 바퀴 반지름의 3.25 배에 해당하는 높이를 가진 장애물을 넘을 수 있었고, 평지에서는 0.7 의 비저항을 유지한 채 초당 로봇의 몸길이의 2.4 배에 해당하는 거리를 주행할 수 있었다.

키워드: 설계, 다리가 달린 바퀴, 이동 수단, 메커니즘, 변신 바퀴.

학번: 2012-20653